Proteomic and phosphoproteomic analyses of Jurkat T-cell treated with 2'3' cGAMP reveals various signaling axes impacted by cyclic dinucleotides.

Kenneth I. Onyedibe[1,2], Rodrigo Mohallem[3,4,], Modi Wang[1], Uma K. Aryal[3,4], Herman O. Sintim[1,2*]

[1]Department of Chemistry, Purdue University, West Lafayette, IN, US
[2]Purdue Institute for Drug Discovery and Purdue Institute of Inflammation, Immunology and Infectious Disease, Purdue University, West Lafayette, IN, US
[3]Department of Comparative Pathobiology, Purdue University, West Lafayette, IN 47907
[4]Purdue Proteomics Facility, Bindley Bioscience Center, Purdue University, West Lafayette, IN, US

*Corresponding author. Email: hsintim@purdue.edu

Abstract

Cyclic dinucleotides (CDNs), such as 2'3'-cGAMP, bind to STING to trigger the production of cytokines and interferons, mainly via activation of TBK1. STING activation by CDN also leads to the release and activation of Nuclear Factor Kappa-light-chain-enhancer of activated B cells (NF-κB) via the phosphorylation of Inhibitor of NF-κB (IκB)-alpha (IκBα) by IκB Kinase (IKK). Beyond the canonical TBK1 or IKK phosphorylations, little is known about how CDNs broadly affect the phosphoproteome and/or other signaling axes. To fill this gap, we performed an unbiased proteome and phosphoproteome analysis of Jurkat T-cell treated with 2'3'-cGAMP or vehicle control to identify proteins and phosphorylation sites that are differentially modulated by 2'3'-cGAMP. We uncovered different classes of kinase signatures associated with cell response to 2'3'-cGAMP. 2'3'-cGAMP upregulated Arginase 2 (Arg2) and the antiviral innate immune response receptor RIG-I as well as proteins involved in ISGylation, E3 ISG15-protein ligase HERC5 and ubiquitin-like protein ISG15, while downregulating ubiquitin-conjugating enzyme UBE2C. Kinases that play a role in DNA double strand break repair, apoptosis, and cell cycle regulation were differentially phosphorylated. Overall, this work demonstrates that 2'3'-cGAMP has a much broader effects on global phosphorylation events than currently appreciated, beyond the canonical TBK1/IKK signaling.

1.0 Introduction

Cyclic dinucleotide (CDN)-mediated Stimulator of Interferon Genes (STING) signaling has emerged as important signaling axes that regulate various processes including cytokine production and autophagy[1-6]. Upon binding to CDN, STING undergoes conformational changes, which promotes its aggregation and enables the phosphorylation of Interferon Regulatory Factor 3 (IRF3) via TANK-binding kinase 1 (TBK1) and release of Nuclear Factor Kappa-light-chain-enhancer of activated B cells (NF-κB)[7, 8]. Recent evidence indicates that beyond the activation of TBK1, CDNs also affect phosphorylation events mediated by other kinases. We recently reported that c-di-GMP promotes Cyclooxygenase-2 (COX-2) expression in STING-independent manner via the TLP2-MEK-ERK pathway[9]. Additionally, we showed in another study that both c-di-GMP and cGAMP upregulate several kinases in RAW macrophage[10]. With the use of kinase inhibitors, it was revealed that STING signaling could be attenuated via Notch signaling[11]. The foregoing illustrates that STING signaling and/or CDN signaling (via STING or non-STING pathways) is more complicated and involves various (yet not fully characterized) signaling pathways, which utilize phosphorylation. In an important study by Koch et al.[12], it was demonstrated that various kinase inhibitors,

including inhibitors of ALK tyrosine kinase receptor (ALK), AMP-activated protein kinase (AMPK), MAP kinase-activated protein kinase 5 (MAPKAPK5), suppressed STING signaling and interferon production in monocyte cell lines[12]. The Koch study provided yet another hint that various kinase signaling and STING signaling intersect to shape the response to intracellular DNA or CDNs. While these prior studies indicate that CDNs affect the phosphoproteome in a broader manner than previously appreciated, we currently do not have detailed characterization of how CDNs affect the phosphoproteome. In T-cells, cGAMP binding to STING leads to myriads of signaling events that includes calcium signaling, interferon production, apoptosis to name a few[13-15]. Since kinase signaling also regulates these processes and there is intersection between STING and other non-TBK1 kinase signaling, we embarked on a project to characterize how cGAMP affects the phosphorylation state of the proteome, using Jurkat T-cell as a model cell.

2.0 Results

2.1 Global proteomics profiling

Cyclic dinucleotides such as 2'3'-cGAMP do not easily permeate cells because they are negatively charged[16]. However, it has been previously observed that CDN concentrations as high as 100 μM can get into cells to activate STING[10, 17, 18]. Recently, it has been shown that 2'3'-cGAMP can get into cells via anion channels such as LRRC8A[19, 20] or solute carrier SLC46A2[21-23]. Thus, we proceeded to treat human Jurkat T-cell with either 100 μM of 2'3'-cGAMP or sterile distilled water (H_2O) and analyzed for changes in the relative abundance levels of their proteomes after 24 h of treatment. An overview of proteomics workflow is shown in **Figure 1**. For global proteomics, a total of 3119 proteins were identified of which >96% were common whereas 76 and 27 proteins were identified only in control and in 2'3'-cGAMP treatment, respectively (**Figure 2A; Tables S1 and S2)**. Scatter, violin, and principal component analysis (PCA) plots (**Figures S1-S2**) showed high correlation between replicates and high reproducibility of the LC-MS analysis.

To establish difference in the protein abundances between 2'3'-cGAMP treated and untreated cells, proteins with p value ≤ 0.05 and Log2 (fold-change) ≥ 0.5, were considered as significantly upregulated by the treatment. Fifty-six proteins were upregulated by 2'3'-cGAMP including 27 proteins (**Table S1**) only identified in 2'3'-cGAMP treated cells **(Table S3)**. Amongst the upregulated proteins were several interferon signaling proteins such as Interferon-induced protein with tetratricopeptide repeats 1, 2, and 3 (IFIT1, IFIT2 and IFIT3); Ubiquitin-like protein ISG15 (ISG15) and, E3 ISG15-protein ligase HERC5 (HERC5). HERC5

was the most upregulated protein (12-fold) in 2'3'-cGAMP treated cells. These proteins are also shown in a Volcano plot (**Figure 2B**). UMP-CMP kinase 2 mitochondrial (CMPK2), a nucleoside monophosphate kinase with immunostimulatory and antiviral functions[24] and Histone H3 were among the top 10 most upregulated proteins in 2'3'-cGAMP treated cells **(Figure S3A**). Arginase 2 (ARG2), Serine/threonine protein phosphatase CPPED1 (CPPED1) and Protein phosphatase 1H (PPM1H) were identified only in the 2'3'-cGAMP treated cells (**Table S1**).

Conversely, a total of 153 proteins were downregulated by 2'3'-cGAMP including 76 proteins (**Table S2**) only identified in the control cells (**Table S4**). Top 10 downregulated proteins are shown in **Figure S3B**. Transport proteins/importins accounted for 8.3% while proteins of ISGylation or ubiquitination, especially E3 ligases accounted for 7.7% of all the significantly downregulated proteins (**Figure S4**, **Table S5**). Kinases such as Serine/threonine protein kinase Nek7 (NEK7), Hexokinase-2 (HK2), SRSF protein kinase 1 (SRPK1), Cyclin-dependent kinase 9 (CDK9), and Serine/threonine protein kinase tousled-like 2 (TLK2) were also identified as downregulated proteins (**Figure S4** and **Tables S5)**.

Ingenuity pathway analysis (IPA) [25] identified Hypercytokinemia/hyperchemokinemia and interferon signaling were amongst the top 20 significantly regulated pathways as shown in **Figure 3** and **Table S6**. The Interferon-induced, double-stranded RNA-activated protein kinase (EIF2AK2), identified as significantly downregulated protein by 2'3'-cGAMP and in the IPA was implicated and enriched in multiple signaling pathways including the hypercytokinaemia, necroptosis, NF-κB, and Toll-like receptor (TLR) pathways (**Table S6).** Histogram plots show positive regulation of intracellular protein kinase cascade (**Figure 3B**) and positive regulation of lymphocyte activation (**Figure 3C**) due to 2'3'-cGAMP treatment.

Gene Ontology (GO) enrichment analysis for biological process using PANTHER [26-28] showed over-representation of genes involved in regulation of type I interferon production with a fold enrichment of 40.54 among the significantly upregulated proteins (p 0.000000143, FDR = 0.00227) and viral penetration into host cells as the most overrepresented GO term among the downregulated proteins with a fold enrichment of >100 **(Table S7).** These findings agreed with the IPA results. Graphical summary of enrichment analysis of ingenuity pathways is shown in **Figure S5**.

Network analysis of significantly upregulated proteins by Metascape[29] showed network of biological processes, including the regulation of transcription and type I interferon production (**Figure S6**), whereas downregulated proteins were categorized into six different MCODE biological processes, such as RNA transport and protein ubiquitination (**Figure S7**).

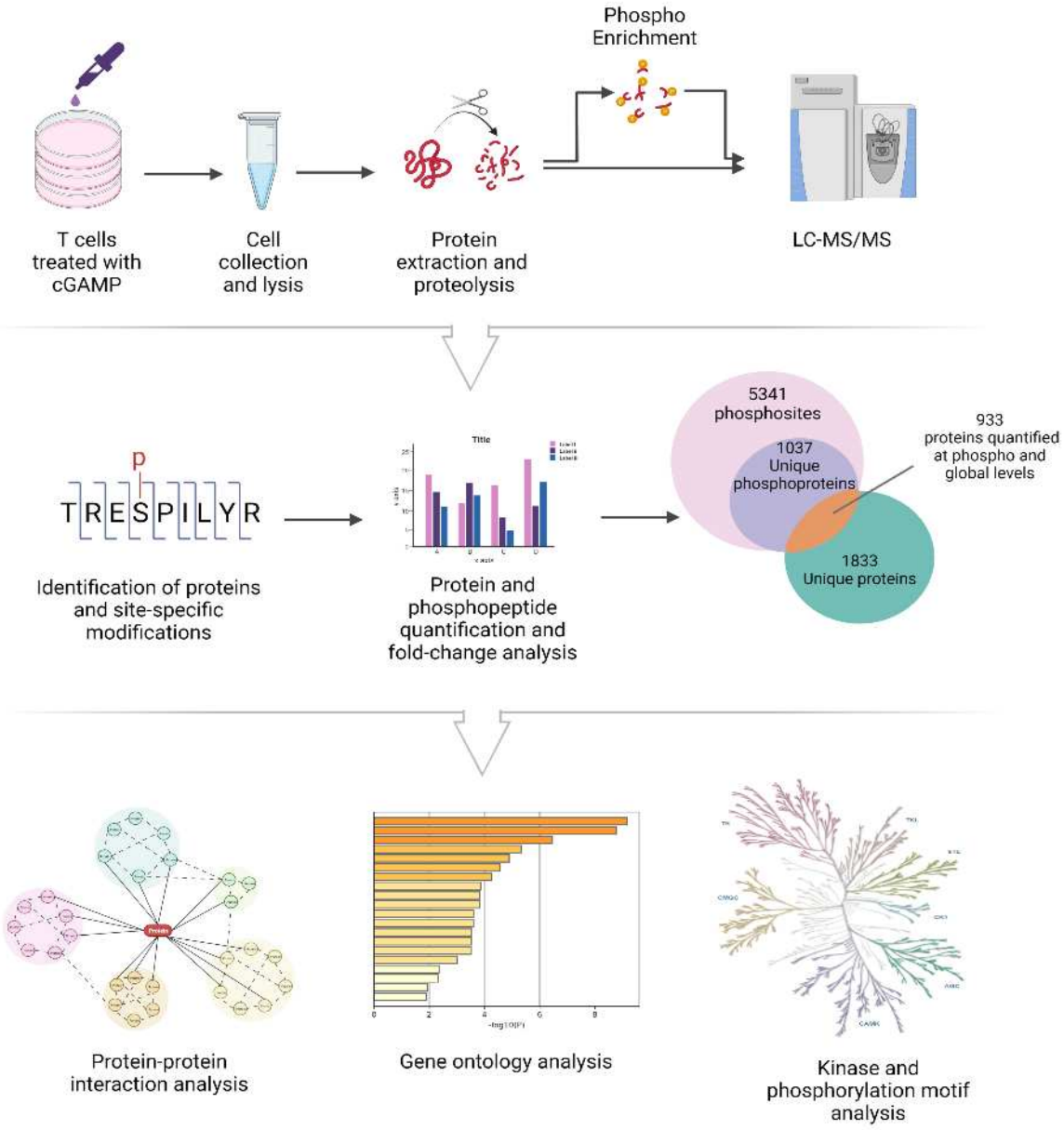

Figure 1: Proteomic profiling of 2'3'-cGAMP treated T-cells. Flow chart of proteomics workflow and summary data. Figure was created with BioRender.com software.

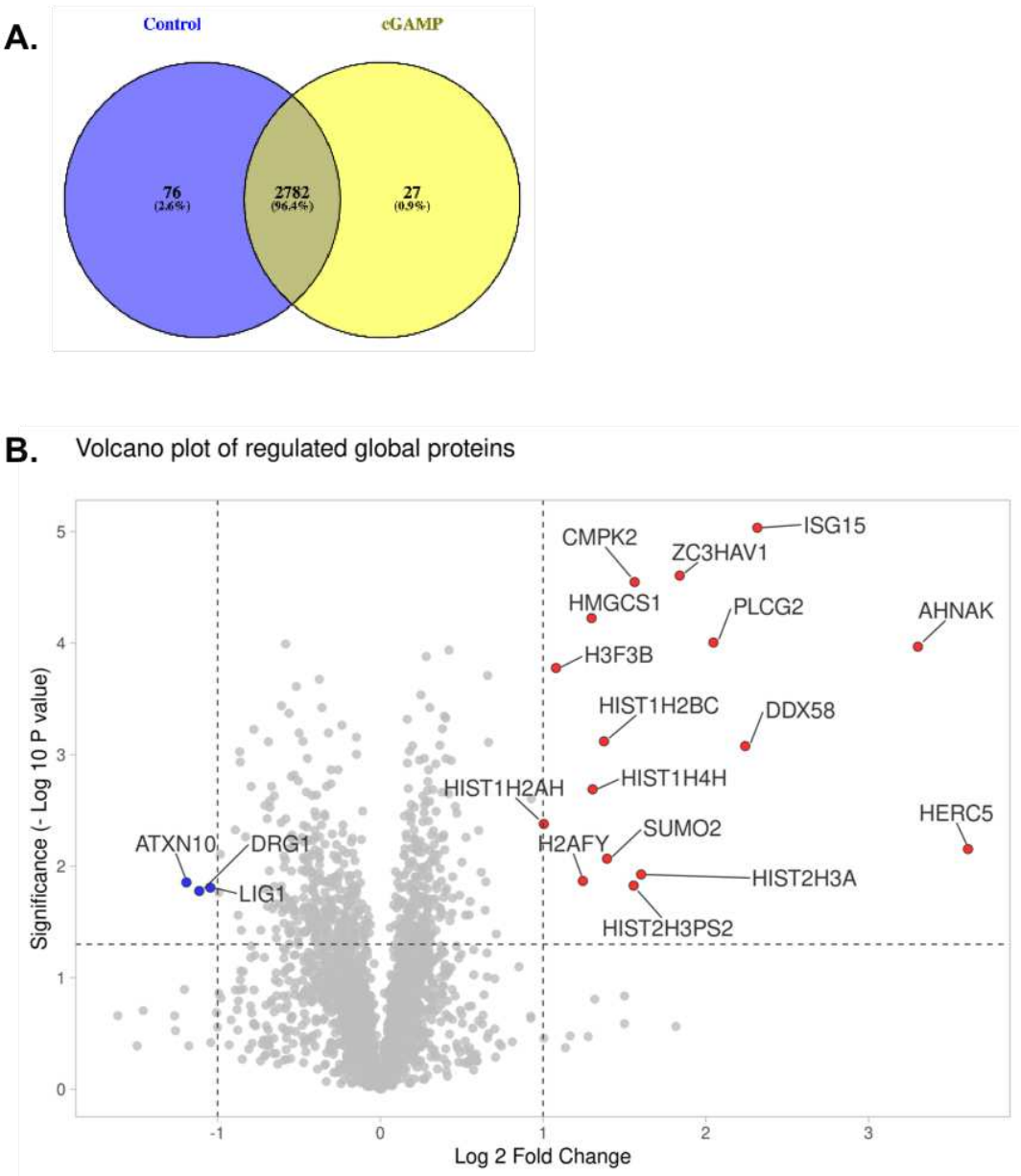

Figure 2: (A) Venn diagram of identified proteins. Out of the 3119 identified global proteins, ~96% were observed in both control and 2'3'-cGAMP treated cells. (B) Volcano plot showing significantly up-(red) or down-(blue) regulated proteins. Volcano plots were plotted using VolcaNoseR software (https://huygens.science.uva.nl/VolcaNoseR).

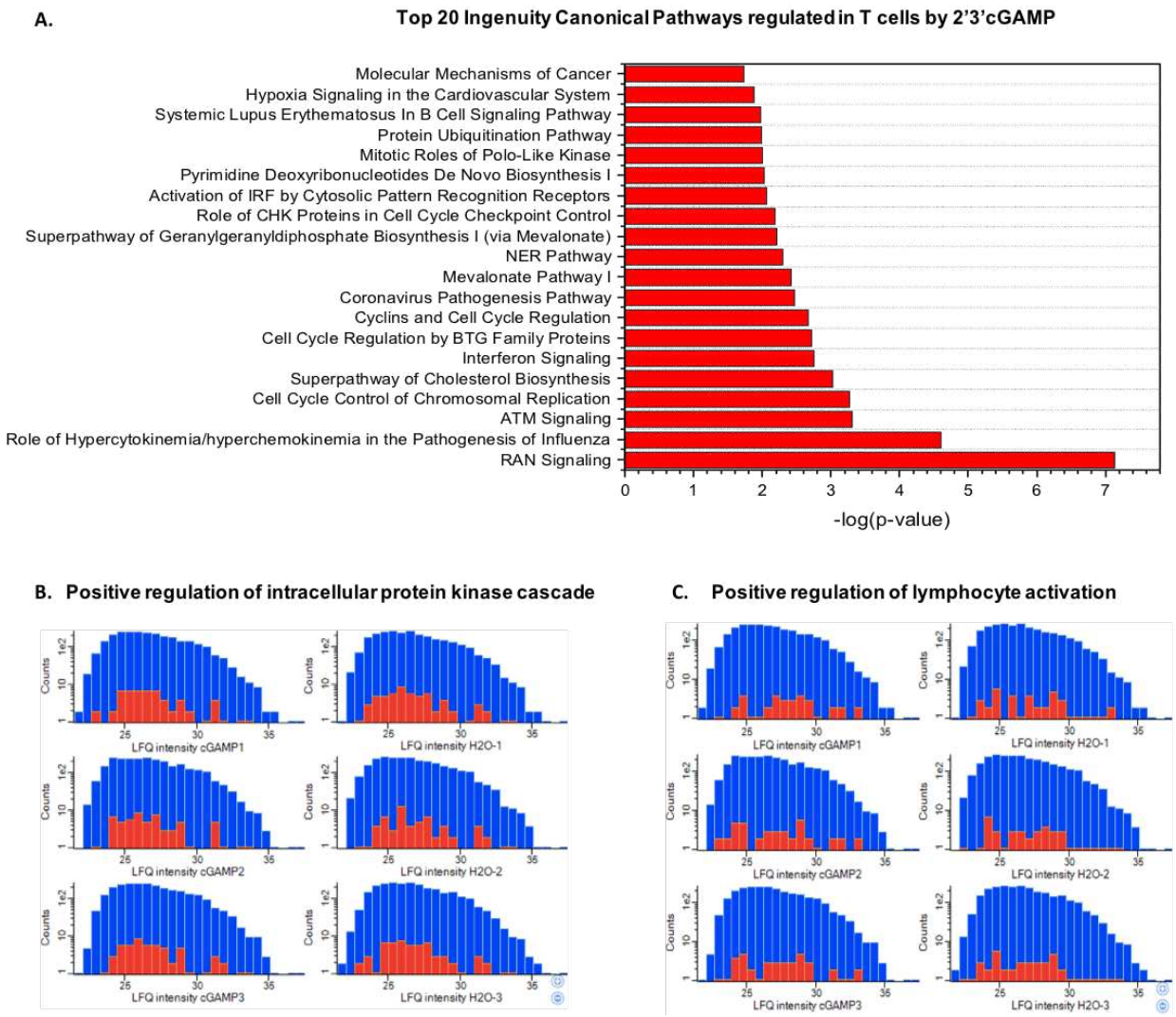

Figure 3: Analysis of biological pathways that are regulated by 2'3'-cGAMP. **(A)** Top 20 pathways regulated by 2'3'-cGAMP. P values represented as -log10 (p-values). Data plotted using Origin (Pro), Version 2020. OriginLab Corporation, Northampton, MA, USA**. (B)** Histogram showing differences in proteins involved in positive regulation of intracellular protein kinase cascade (red bars) in 2'3'-cGAMP treated versus control cells. **(C)** Histogram showing differences in proteins involved in positive regulation of lymphocyte activation (red bars) in 2'3'-cGAMP treated versus control cells. Histograms were plotted using Perseus software.

2.2 Phosphoproteome analysis

Protein phosphorylation alters protein function, localization, and protein activity, depending on the specific residue that was modified[30]. The identified phosphopeptides dataset was first filtered based on class I phospho STY sites, defined as sites with a localization probability greater than 0.75 (75%), resulting in 5341 quantified phosphosites, from which 294 sites were differentially regulated ($p \leq 0.05$) between the treatment and control groups. Among the 5341 class I phosphosites, 69 phosphosites were not found in the curated Phosphosite Plus database **(Table S8)**. These new phosphorylation sites were observed in IFIT3 at

S24 (26-fold up in 2'3'-cGAMP treated cells) and in protein TIMELESS at S446 (16-fold lower in the treated cells). Other new phosphosites belong to DNA topoisomerase 2-beta (TOP2B), AHNAK, Tyrosine-protein kinase Lck (LCK), and SFRS2 protein (SFRS2). TOP2B was approximately 2-3-fold more phosphorylated at S227, S265, S318, S378, and S433 in 2'3'-cGAMP treated T-cell. Visualization of differentially regulated phosphosites into a heatmap by hierarchical clustering (**Figure 4A**) showed two distinct clusters evenly distributed between up- and downregulated phosphosites.

Gene Ontology (GO) enrichment analysis of the downregulated phosphoproteins identified enrichment of proteins involved in RNA processing, DNA maintenance and cell cycle progression among the top GO-BP terms (**Figure 4B)**. Interestingly, such processes were also enriched in upregulated phosphoproteins (**Figure 4C**), suggesting that cellular response to 2'3'-cGAMP treatment is dependent on specific proteins. Notably, phosphorylation of Cyclin-dependent kinase (CDK) 11 at S566 was > 9-fold lower in 2'3'-cGAMP treated cells compared to control cells. Similarly, phosphorylation of other cell cycle or leukocyte associated proteins at various phosphosites such as Phosphatidylinositol 4-kinase beta (PI4KB)-S523, Tyrosine-protein kinase ZAP-70 (ZAP70)-T494, Proto-oncogene tyrosine-protein kinase Src (SRC)-S75, SH3 domain-containing kinase-binding protein 1 (SH3KBP1)-S183, and Ubiquitin carboxyl-terminal hydrolase 36 (USP36)-S442 were 4-8 folds lower in 2'3'-cGAMP treated T-cells compared to control T-cells. On the other hand, phosphorylation of proteins such as IFIT3 at S24 and S299 were 22-60-fold higher in 2'3'-cGAMP treated cells compared to control cells. Also, phosphorylation of Neuroblast differentiation-associated protein AHNAK (AHNAK) at S135, S210, S216 and S5752 were 4-16-fold higher in 2'3'-cGAMP treated cells compared to control T-cells. See **Table S9** for a list of all 294 differentially phosphorylated sites ($p < 0.05$).

We further categorized these differentially regulated phosphoproteins according to their STRING database biological functions **Table S10**. Proteins involved in autophagy, myeloid cell differentiation, regulation of double strand break repair, nuclear excision repair (NER), RAN binding domain and interferon signaling were amongst the differentially phosphorylated targets in 2'3'-cGAMP treated compared to control T-cells.

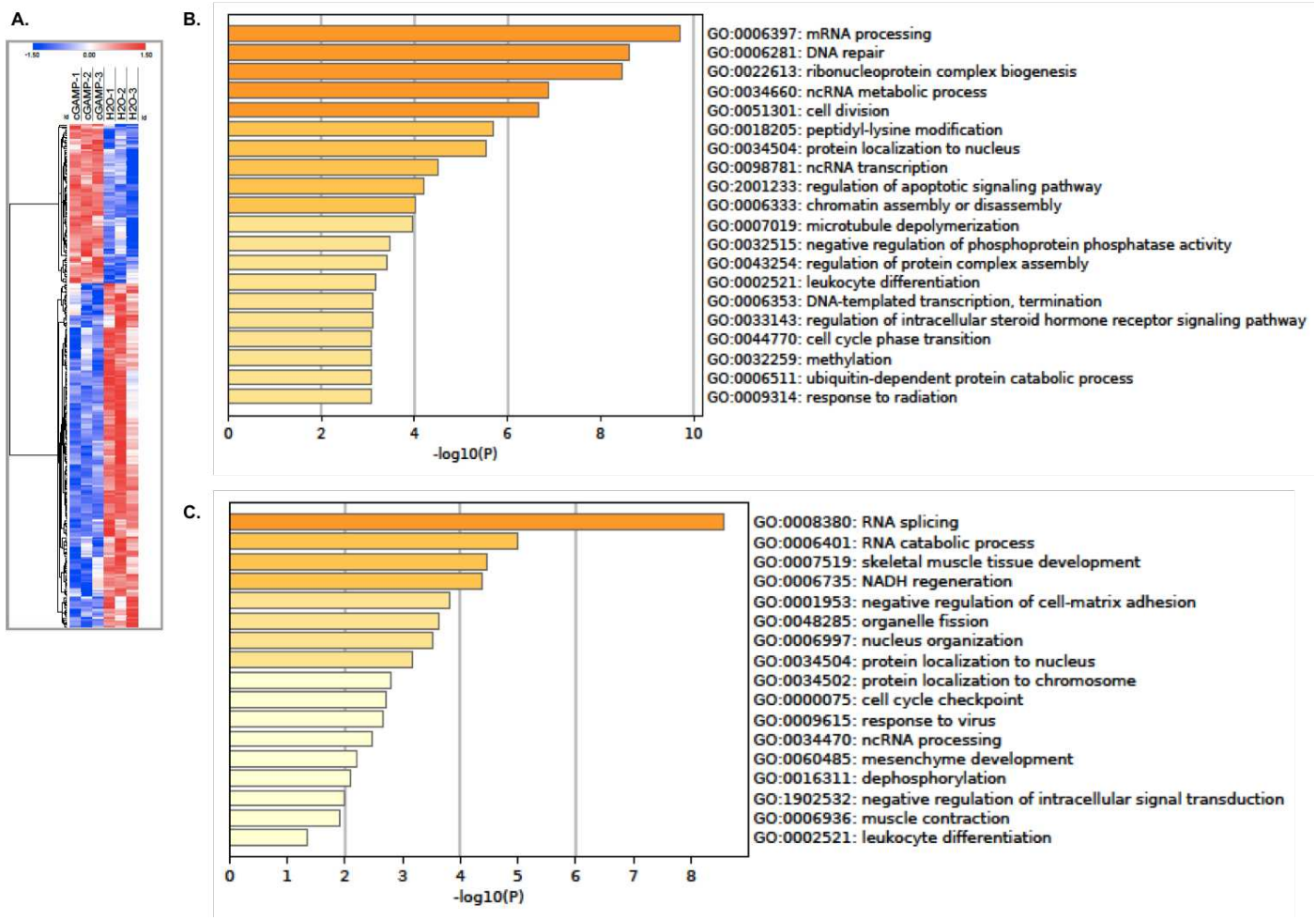

Figure 4: Heatmap with hierarchical clustering in two distinct groups of differentially phosphorylated phosphosites following phospho- proteomics analysis. (B) Distinct Gene Ontology – Biological Process (GO-BP) terms significantly enriched from all significantly downregulated phosphoproteins. (C) Distinct GO-BP terms significantly enriched from all significantly upregulated phosphoproteins.

Protein phosphorylation also modulates protein-protein interactions[31]. To map putative protein-protein interactions of significant phosphoproteins, we performed interactome analysis using the metascape software[29]. The downregulated phosphoproteins were enriched for mRNA processing, regulation of gene expression and cell cycle regulation**.** Regulation of nucleic acid metabolism and glucose metabolism were evident amongst the upregulated proteins. Cytoscape was used to illustrate interaction network of the downregulated phosphoproteins[32] (**Figure 5**).

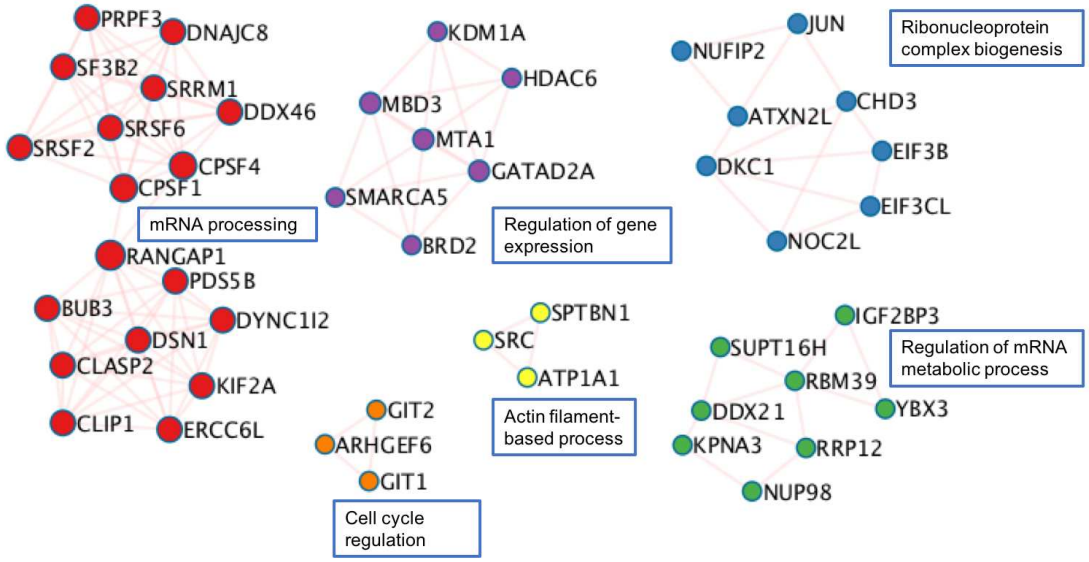

Figure 5: Protein-protein interaction networks of downregulated phosphorylated proteins. Figure made on Cytoscape software.

2.3 Differentially phosphorylated kinases and phosphatases and kinase motif profiling

With the observation of many differentially phosphorylated proteins and phophosites, we sought to understand the kinase groups and motifs that drive these phosphorylation events and used the cell signaling technology-mapping tool to create a kinase tree of the differentially regulated kinases. TKL, STE, TK, CMGC, CK1, AGC, and CAMK kinase were the most impacted families by 2'3'-cGAMP treatment (**Figure 6A)**. Similar kinase families were also found in the kinase tree analysis using the differentially quantified global proteins (**Figure S8**). Protein phosphatase 1H (PPM1H) was differentially phosphorylated at position S211 following the 2'3'-cGAMP treatment. There were no differences in total proteins for LCK and SH3KBP1 between the treated and untreated samples, but they were differentially phosphorylated at Y454 and S183, respectively. The most significantly regulated kinases and phosphatases with a localization probability of >0.9 (90-100%) are shown in **Table 1**.

NetPhorest kinase motif analysis, which predicts kinase specificity based on the motifs surrounding the phosphorylated site mapped in our phosphoproteomic analysis, suggested that most of the differential kinase motifs were in the Casein kinase II (CK2), the Cyclin dependent kinases (CDK) 1/2/3/5 and the Mitogen activated protein kinase (MAPK) 1/3/7 groups (**Figure 6B**). A kinase motif enrichment analysis showed that the most significantly enriched motifs were G protein-coupled receptor kinase 1, Glycogen

synthase kinase-3 (GSK3), protein kinase A (PKA) and protein kinase C (PKC) substrate motifs. Other motifs such as 14-3-3 and Bromodomain substrate motifs were also impacted by 2'3'-cGAMP treatment.

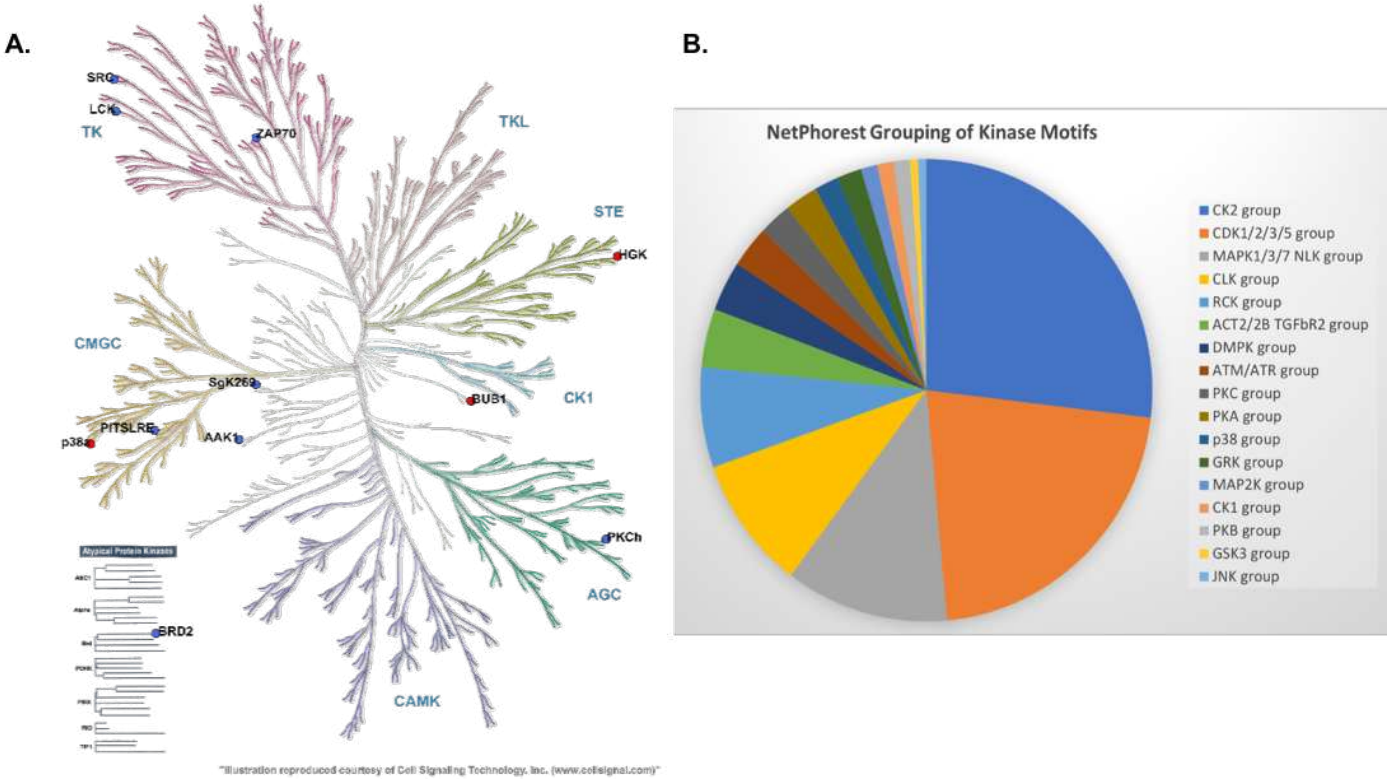

Figure 6: **(A)** Kinase tree map of regulated kinases following phosphoproteomics analysis.

TKL = Tyrosine kinase like; STE = serine/threonine kinases; TK = Tyrosine kinase; CMGC = represents the initials of members of the subfamily: cyclin-dependent kinase (CDK), mitogen-activated protein kinase (MAPK), glycogen synthase kinase (GSK) and CDC-like kinase (CLK)); CK1 = Casein kinase; AGC = represents the last letters of cAMP-dependent protein kinase (PKA), the cGMP-dependent protein kinase (PKG) and the protein kinase C (PKC) families; and CAMK = calcium/calmodulin-dependent kinases. This figure is courtesy of cell signaling technology Inc. (www.cellsignal.com) **(B)** NetPhorest Grouping of Kinase Motifs showing most impacted kinase motifs.

Table 1: Differentially phosphorylated kinases and phosphatases in treated vs control T-cells (90 -100% localization probability, P <0.05, Log 2-fold change > ± 0.5)

S/No.	Kinase/Phosphatase	Gene names	Amino Acid	Position	Localization probability	p-value	Log 2 Fold Change
1	Cyclin-dependent kinase 11B; Cyclin-dependent kinase 11A	CDK11B; CDK11A	S	566	1	0.005	-3.18
2	SH3 domain-containing kinase-binding protein 1	SH3KBP1	S	183	1	0.026	-2.91
3	Serine/threonine-protein phosphatase 6 regulatory subunit 1	PPP6R1	S	635	1	0.001	-2.86
4	Serine/threonine-protein phosphatase 6 regulatory subunit 1	PPP6R1	S	638	1	0.002	-2.73
5	Phosphatidylinositol 4-kinase beta	PI4KB	S	523	1	0.034	-2.19
6	Pseudopodium-enriched atypical kinase 1	PEAK1	S	281	1	0.044	-0.64
7	Tyrosine-protein kinase Lck	LCK	Y	454	1	0.023	-0.6
8	Protein kinase C eta type	PRKCH	S	675	1	0.02	-0.59
9	Protein phosphatase 1H	PPM1H	S	211	1	0.038	2.38
10	Proto-oncogene tyrosine-protein kinase Src	SRC	S	75	0.99	0.005	-2.72
11	Mitotic checkpoint serine/threonine protein kinase BUB1	BUB1	S	596	0.99	0.036	0.99
12	Serine/threonine-protein kinase 11-interacting protein	STK11IP	S	366	0.98	0.026	-1.64
13	AP2-associated protein kinase 1	AAK1	T	606	0.98	0.042	-0.67
14	52 kDa repressor of the inhibitor of the protein kinase	PRKRIR	S	141	0.95	0.047	-2.59
15	Tyrosine-protein kinase ZAP-70	ZAP70	T	494	0.91	0.034	-1.99

2.6 Immunoblot validation of differentially regulated proteins

To validate the results of the proteomics and phosphoproteomics analyses, we performed Western blot analysis of lysates collected after 24 h treatment with 2'3'-cGAMP for several representative proteins (**Figure 7**). Up-regulation of HERC5, DDX58, ZC3HAV1, SUMO4, H3 and ISG15 as determined by

proteomic analysis was corroborated by WB. ARG2 which was identified in the 2'3'-cGAMP treated cells only in the proteomics analysis also showed similar pattern when immunoblotted **(Figure 7A**). Similarly, UBE2C, detected only in control T-cells in the proteomics analysis (**Table S2**) also showed a similar pattern in the immunoblots, further validating proteomics results and its downregulation by 2'3'-cGAMP (**Figure 7A**).

Recently, asides phosphorylation, the role of unconventional post translational modifications in cGAS-cGAMP-STING mediated signaling has generated significant interest[33]. Whereas ubiquitylation is known to play important roles in this signaling axis, ISGylation regulated by cGAMP in T-cells has not yet been shown. ISGylation occurs when ISG15 is conjugated to target proteins[34]. Our data show that ISG15 and HERC5 (ISG15 E3 ligase), major players in ISGylation were amongst the highest upregulated proteins. We demonstrated that cGAMP treated cells showed marked differences in ISG15 conjugated proteins when compared to controls (**Figure 7C**).

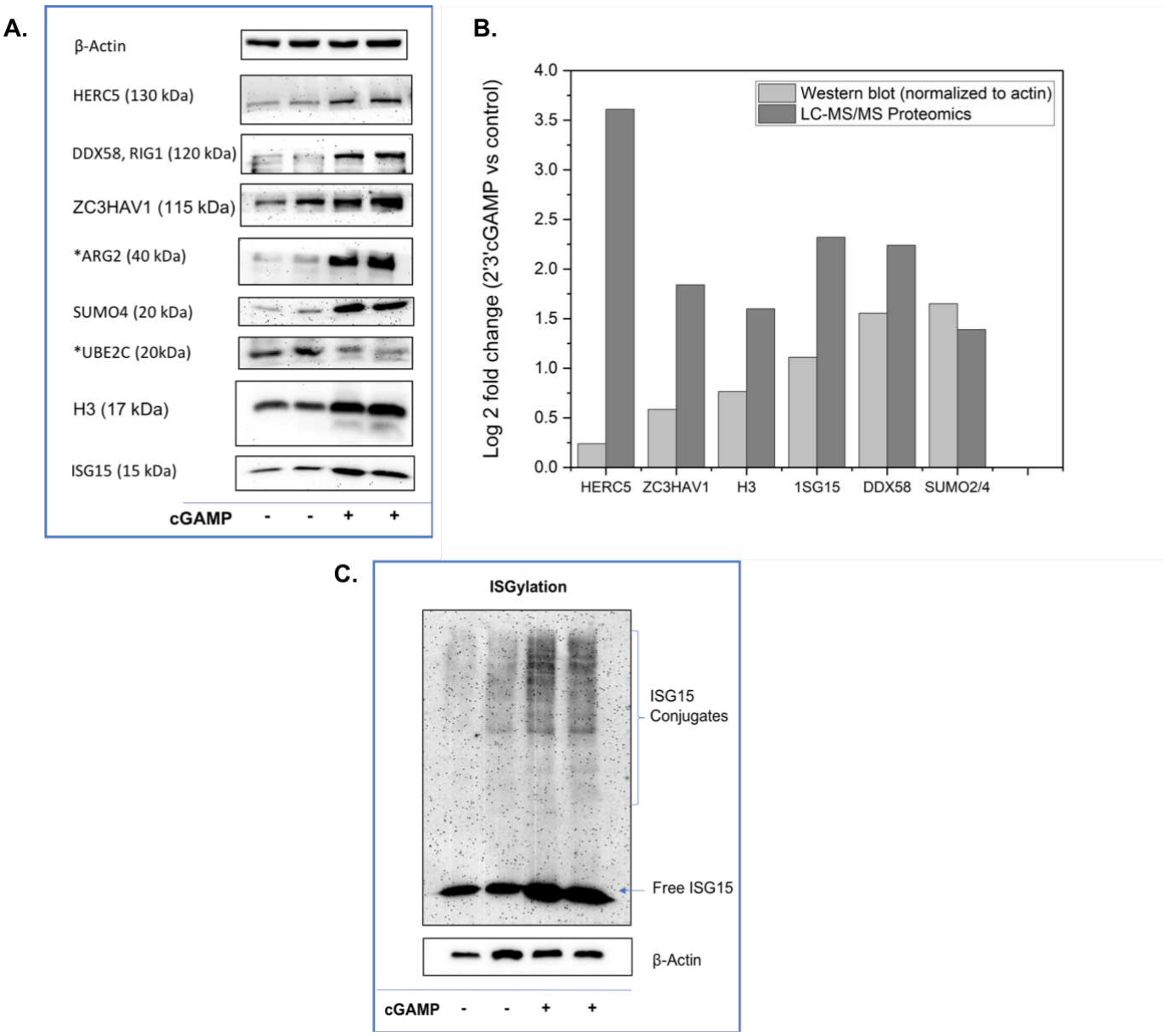

Figure 7: Immunoblot validation of selected differentially regulated proteins. **(A)** Western blot images of differentially regulated proteins in treated (100 µM 2'3'cGAMP, 24 h) vs untreated. *For LC-MS/MS data, ARG2 was below detectable limits in the control samples while *UBE2C was below detectable limits in the 2'3'cGAMP treated samples. Blot images shown for ARG2 and UBE2C were for both treated and control samples. **(B)** Log 2-fold change of blot intensity from densitometric analysis normalized to B-Actin compared with the LC-MS/MS LFQ log 2-fold change of cGAMP treated samples vs untreated controls. Original blot images are shown in Figure S9. **(C)** 2'3'-cGAMP mediated ISGylation in T-cells. Immunoblot showing proteins conjugated to ISG15 (ISGylation) and free ISG15 with and without treatment with 2'3'-cGAMP (24 h). Original blot image is shown in Figure S10

3.0 Discussion

T-cell signaling is known to be a major link between the innate and adaptive immune responses[35]. On the other hand, the cGAMP-STING pathway has been extensively studied as critical modulators of the

innate immune response[36]. We chose Jurkat T-cell for our study because this cell line is easy to maintain, which had previously been used to demonstrate the effects of c-di-GMP on mammalian cells[37] as well as cGAMP[13]. Indeed, high levels of cGAMP in T-cells (produced under conditions that release DNA into the cytosol, such as oxidative damage or via DNA damaging agents) have been shown to cause apoptosis[14]. Proteome profiling of T-cells treated with 2'3'-cGAMP showed similar response to what has been previously reported in innate immune cells such as macrophages[10, 38]. For example, ISG15, a central modulator of host immune response through its conjugation to a target protein in a process called ISGylation, or as a free protein, was significantly upregulated in 2'3'-cGAMP treated T-cells, as has been shown in macrophages[10, 13, 38]. Additionally, it is known that ISG15 upregulation increases the secretion of IFN-γ and cGAMP also seem to enhance the expression of ISGylation related proteins such as ISG15 and HERC5[34]. ISG15 during ISGylation is conjugated to a lysine of target protein, in a reaction catalyzed by E1 (activating), E2 (conjugating), and E3 (ligating) enzymes[39]. Four of these E3 enzymes (HERC5, TRIM25, TRIM26 and RNF220) were also significantly upregulated by 2'3'-cGAMP in this study. Additionally, IFIT1 and DDX58, previously reported as ISGylation targets[40] were also upregulated by 2'3'-cGAMP. We demonstrate for the first time, 2'3'-cGAMP mediated conjugation of ISG15 to target proteins in T-cells. Campbell and colleagues have previously shown that the free form of ISG15 stimulated natural killer (NK) cell proliferation, neutrophil chemotaxis and IFN-gamma production by T-cells, inducing further activation of monocytes and NK cells[41]. Other upregulated proteins such as DDX58 (RIG-1), 2'-5'-oligoadenylate synthase-like protein (OASL) and 2'-5'-oligoadenylate synthase 2 (OAS2) are known sensors of cytosolic RNA[42] and play active roles in immunity against *Mycobacterium tuberculosis* (Mtb) and inhibit intracellular Mtb replication[43, 44]. The impact of 2'3'-cGAMP on T-cells and immune response was clearly evident from the upregulation of proteins that play critical roles in ISGylation, immune sensing and interferon signaling.

On the other hand, differential modulation of RB1, SRC, CDK9, CDK11 and BUB1suggested an impact of 2'3'-cGAMP treatment on cell cycle associated pathways (**Figure 2A**, **3B, 3C, 4A**) and kinase motifs (**Figure 3E**). RB1 dephosphorylation at T821 is required for cells to undergo apoptosis, and exposure to cGAMP is known to cause apoptosis[14, 45]. RB1-T821 phosphorylation was ~ 2-fold lower in treated cells compared to controls (**Figure 7A**; **Table S9 (SI in Excel)**. Also, phosphorylation of SRC at S75, a protein-tyrosine kinase important in cell growth, cell division, and migration, and cellular survival signaling pathways was downregulated ~ 8-fold by 2'3'-cGAMP treatment[46]. Earlier reports show that phosphorylation of SRC at S75 promotes ubiquitylation and degradation of active SRC thereby limiting its

activity[47]. Thus, decreased phosphorylation of SRC at S75 increases the activity of SRC. Additionally, CDK1 and CDK5 have been shown to phosphorylate SRC at S75[48]. Moreover, phosphorylation of the mitotic check point protein BUB1 at S596 was ~2 fold higher whilst that of CDK11 at S566 was ~ 9-fold lower in cGAMP treated cells (See **Table 1**). It is currently not known how phosphorylation of BUB1 at S596 or CDK11 at S566 affect function and future work is needed to clarify these issues. The ability of T-cells to link the innate and adaptive immune response is mediated by the T-cell receptor (TCR)[35]. The activation of TCR enables the recognition of peptides bound to major histocompatibility complex (MHC) molecules[49] and stimulates signaling cascades that culminates in specific adaptive immune and innate responses[35]. Many proteins involved in TCR signaling including DNA-dependent protein kinase catalytic subunit (PRKDC) and DNA repair protein XRCC4 (XRCC4) were differentially phosphorylated after 2'3'-cGAMP treatment at S2612 and S318, respectively. PRKDC phosphorylation at S2612 is important for precise end joining during DNA double strand break repair[50, 51]. Thus, PRKDC is a critical kinase for nonhomologous end-joining (NHEJ) of DNA during V(D)J recombination. Differential upregulation of LCK phosphorylation at Y454 (newly reported site) and downregulation of ZAP70 at T494 may be important for TCR regulation[49], however biological implications of their differential phosphorylation are yet to be elucidated.

Phosphoproteomic analysis revealed a dual phosphorylation of PPM1H at S123 and S211 in 2'3'-cGAMP treated cells, but not in control T-cells. Osawa et al. recently showed that PPM1H phosphorylation at these two positions via cAMP-dependent protein kinase (PKA) and Ca2+/calmodulin-dependent protein kinase I (CaMKI) regulate dephosphorylation of Mothers Against Decapentaplegic Homolog1 (SMAD1) [52]. SMAD1 is a PPM1H substrate which functions as a transcription factor implicated in Transforming growth factor beta (TGF-β) and bone morphogenic protein (BMP) signaling[53-55]. On the other hand, AHNAK potentiates TGF-β signaling and negatively regulate cell growth [56]. AHNAK was upregulated ~10 fold and differentially phosphorylated at multiple positions in the 2'3'-cGAMP treated T-cells in this study (**Figure S3 and Table S2**)

4.0 Conclusion

Inflammation is an important cellular process of the host immune response to pathogens. We have shown that 2'3'-cGAMP play an important role in modulating the abundances of proteins and phosphoproteins involved in ISGylation, regulation of type I interferons, regulation of cell cycle and DNA repair. Previously, there was little information about 2'3'-cGAMP triggered phosphorylation events and

related kinases in T-cells. This study fills that gap and suggests regulation of several kinases such as BUB1, PRKCH, PRKDC, ZAP70, LCK, and SRC in the presence of 2'3'-cGAMP in T-cells. Furthermore, 2'3'-cGAMP treatment impacted critical kinase motifs including CK2, CDK 1/2/3/5, MAPK 1/3/7, GSK3, PKA and PKC motif groups, likely suggesting multiple host defense mechanism against pathogens. This work demonstrates that beyond the canonical TBK1 and IKK kinases, 2'3'-cGAMP broadly affects many other kinases signaling axes. The immediate goal of this study was to reveal that cGAMP has a much broader effects on global phosphorylation, beyond the canonical TBK1/IKK signaling using an unbiased proteomics approach. A limitation of the present study is that Jurkat cells, although useful as a model of T cells, might not completely recapitulate the response to CDNs by normal T cells in vivo. Future work will investigate other cell types. Also, in this study, we used 100 μM cyclic dinucleotides and performed a 24 h treatment of the cells. Earlier studies had shown that although 2'3'-cGAMP has poor cellular permeability due to the negative charges, 100 μM, was adequate to cause cytokine release from immune cells after 24 h [10, 66]. CDNs are being evaluated as immunomodulatory agents and depending on dosing, some immune cells may encounter concentrations as high as 100 μM. But for 24 h treatment, the reported effects of 2'3'-cGAMP on Jurkat cells may not reflect initial response to cyclic dinucleotides. Future studies, beyond the scope of the current study, evaluating different time points/concentrations of CDNs and using different cell types, are therefore needed to fill in some of these missing gaps.

Methods

Jurkat T cell lines (ATCC) were grown in RPMI media with 10% fetal bovine serum (FBS) plus antibiotics (100 IU/mL penicillin and 100 μg/mL streptomycin) at 37 °C and 5% CO2 until at least 80% confluency was achieved. For each experiment, cells were seeded in triplicates and grown for 24 h before treating with 100 μM of 2'3'-cGAMP or sterile water (controls) for 24 h before sample collection. Proteomic analysis was performed at the Purdue Proteomics Facility (PPF) as described previously[57]. Briefly, cells collected were lysed in 100 mM ammonium bicarbonate (ABC) in a Barocycler (PBI Inc.) (4 °C, for 90 cycles of 20 s at 35 kPSI and 10 s at 1 ATM) and followed by acetone precipitation at –20 °C overnight. Proteins were reconstituted in 8M urea for processing as previously described[58]. 20 ug of protein were saved for global analysis, and the remainder was enriched for phosphopeptides using the Spin-Tip PolyMAC Phosphopeptide Enrichment kit (Tymora Analytical, IN, USA) as described previously[59, 60]. LC-MS/MS data was collected on a Thermo Q Exactive Orbitrap HF mass spectrometer coupled with a Dionex UltiMate

3000 HPLC system with the use of a 120 min LC gradient. For protein identification and MS quantitation from the raw Mass spectrometry data, we used MaxQuant (version 1.6.3.3)[61].

MaxQuant results were further analyzed in Perseus software[62]. Only proteins identified in a minimum of two out of three treatment replicates and with at least two MS/MS counts were included in all analysis. We performed differential expression analysis of proteins and phosphoproteins using LFQ and STY site intensities. Thus, Log2 transformed LFQ intensities and Student's t-test were used to determine differential abundances. PhosphoSite plus[63], and NetPhorest[64] were used for deeper specific phosphorylation sites analysis while Gene Ontology and PANTHER were used for Gene Ontology analysis[26, 28, 65]. For correlation between replicates, we used Scatter plots and Violin box plots while Venny 2.1 software was used to plot Venn diagrams. Auto-scale normalized data was used for hierarchical clustering and heatmaps while pathway enrichment was carried out using the ingenuity pathway analysis software[25].

Western blotting was completed as reported previously with minor modifications[10]. Specifically, ~1million cells/mL Jurkat T-cells were treated with 100 μM 2'3'-cGAMP or sterile water for 24 h. The cells were lysed in mPER lysis buffer plus inhibitor cocktail and incubated on ice before collection by centrifugation at 19 000 rpm for 10 min at 4 °C. Samples were separated by SDS-PAGE and transferred to nitrocellulose blotting membrane at 100 V for 120 min. 5% Bovine Serum Albumin. (BSA) was used for blocking and antibody preparation. Membranes were analyzed with specific antibodies against ISG15, HERC5, DDX58, UBE2C, ARG2, H3, ZC3HAV1, SUMO4, pRB1-T821 and β-Actin. Antibodies for ISG15 (A1182), HERC5 (A14889), DDX58 (A0550), UBE2C (A5499), ARG2 (A6355), H3 (A2348), ZC3HAV1 (A9219), SUMO4 (A3100), and β-Actin (AC006) were obtained from Abclonal whereas antibody for pRB1-T821 (ab4787) was obtained from Abcam.

5.0 Data Availability

Raw LC-MS/MS data for this study has been deposited in the Mass Spectrometry Interactive Virtual Environment (http://massive.ucsd.edu) with the ID: MSV000088715

6.0 Funding: Funds from NSF grant 2004102 were used for this project.

7.0 References

[1] Zhang, X., Bai, X. C., Chen, Z. J., Structures and Mechanisms in the cGAS-STING Innate Immunity Pathway. *Immunity* 2020, *53*, 43-53.
[2] Li, T., Chen, Z. J., The cGAS-cGAMP-STING pathway connects DNA damage to inflammation, senescence, and cancer. *J Exp Med* 2018, *215*, 1287-1299.
[3] Cheng, W. Y., He, X. B., Jia, H. J., Chen, G. H.*, et al.*, The cGas-Sting Signaling Pathway Is Required for the Innate Immune Response Against Ectromelia Virus. *Front Immunol* 2018, *9*, 1297.
[4] Khoo, L. T., Chen, L. Y., Role of the cGAS-STING pathway in cancer development and oncotherapeutic approaches. *EMBO Rep* 2018, *19*.
[5] Ablasser, A., Chen, Z. J., cGAS in action: Expanding roles in immunity and inflammation. *Science* 2019, *363*.
[6] Cheng, Z., Dai, T., He, X., Zhang, Z.*, et al.*, The interactions between cGAS-STING pathway and pathogens. *Signal Transduct Target Ther* 2020, *5*, 91.
[7] Balka, K. R., Louis, C., Saunders, T. L., Smith, A. M.*, et al.*, TBK1 and IKKε Act Redundantly to Mediate STING-Induced NF-κB Responses in Myeloid Cells. *Cell Rep* 2020, *31*, 107492.
[8] Yum, S., Li, M., Fang, Y., Chen, Z. J., TBK1 recruitment to STING activates both IRF3 and NF-κB that mediate immune defense against tumors and viral infections. *Proc Natl Acad Sci U S A* 2021, *118*.
[9] Wang, M., Chaudhuri, R., Ong, W. W. S., Sintim, H. O., c-di-GMP Induces COX-2 Expression in Macrophages in a STING-Independent Manner. *ACS Chem Biol* 2021, *16*, 1663-1670.
[10] Sooreshjani, M. A. G., Ulvi K. Aryal, Uma K. Sintim, Herman, Proteomic analysis of RAW macrophages treated with cGAMP or c-di-GMP reveals differentially activated cellular pathways. *RSC Adv* 2018, *8*.
[11] Long, J., Yang, C., Zheng, Y., Loughran, P.*, et al.*, Notch signaling protects CD4 T cells from STING-mediated apoptosis during acute systemic inflammation. *Sci Adv* 2020, *6*.
[12] Koch, P. D., Miller, H. R., Yu, G., Tallarico, J. A.*, et al.*, A High Content Screen in Macrophages Identifies Small Molecule Modulators of STING-IRF3 and NFkB Signaling. *ACS Chem Biol* 2018, *13*, 1066-1081.
[13] Larkin, B., Ilyukha, V., Sorokin, M., Buzdin, A.*, et al.*, Cutting Edge: Activation of STING in T Cells Induces Type I IFN Responses and Cell Death. *J Immunol* 2017, *199*, 397-402.
[14] Gulen, M. F., Koch, U., Haag, S. M., Schuler, F.*, et al.*, Signalling strength determines proapoptotic functions of STING. *Nat Commun* 2017, *8*, 427.
[15] Wu, J., Chen, Y. J., Dobbs, N., Sakai, T.*, et al.*, STING-mediated disruption of calcium homeostasis chronically activates ER stress and primes T cell death. *J Exp Med* 2019, *216*, 867-883.
[16] Su, T., Zhang, Y., Valerie, K., Wang, X. Y.*, et al.*, STING activation in cancer immunotherapy. *Theranostics* 2019, *9*, 7759-7771.
[17] Onyedibe, K. I., Elmanfi, S., Aryal, U. K., Könönen, E.*, et al.*, Global proteomics of fibroblast cells treated with bacterial cyclic dinucleotides, c-di-GMP and c-di-AMP. *J Oral Microbiol* 2022, *14*, 2003617.
[18] Chang, D., Whiteley, A. T., Bugda Gwilt, K., Lencer, W. I.*, et al.*, Extracellular cyclic dinucleotides induce polarized responses in barrier epithelial cells by adenosine signaling. *Proc Natl Acad Sci U S A* 2020, *117*, 27502-27508.
[19] Lahey, L. J., Mardjuki, R. E., Wen, X., Hess, G. T.*, et al.*, LRRC8A:C/E Heteromeric Channels Are Ubiquitous Transporters of cGAMP. *Mol Cell* 2020, *80*, 578-591.e575.

[20] Zhou, C., Chen, X., Planells-Cases, R., Chu, J.*, et al.*, Transfer of cGAMP into Bystander Cells via LRRC8 Volume-Regulated Anion Channels Augments STING-Mediated Interferon Responses and Anti-viral Immunity. *Immunity* 2020, *52*, 767-781.e766.
[21] Ritchie, C., Cordova, A. F., Hess, G. T., Bassik, M. C., Li, L., SLC19A1 Is an Importer of the Immunotransmitter cGAMP. *Mol Cell* 2019, *75*, 372-381.e375.
[22] Cordova, A. F., Ritchie, C., Böhnert, V., Li, L., Human SLC46A2 Is the Dominant cGAMP Importer in Extracellular cGAMP-Sensing Macrophages and Monocytes. *ACS Cent Sci* 2021, *7*, 1073-1088.
[23] Luteijn, R. D., Zaver, S. A., Gowen, B. G., Wyman, S. K.*, et al.*, SLC19A1 transports immunoreactive cyclic dinucleotides. *Nature* 2019, *573*, 434-438.
[24] Liu, W., Chen, B., Chen Li, Yao, J.*, et al.*, Identification of fish CMPK2 as an interferon stimulated gene against SVCV infection. *Fish Shellfish Immunol* 2019, *92*, 125-132.
[25] Krämer, A., Green, J., Pollard, J., Tugendreich, S., Causal analysis approaches in Ingenuity Pathway Analysis. *Bioinformatics* 2014, *30*, 523-530.
[26] Ashburner, M., Ball, C. A., Blake, J. A., Botstein, D.*, et al.*, Gene ontology: tool for the unification of biology. The Gene Ontology Consortium. *Nat Genet* 2000, *25*, 25-29.
[27] Consortium, G. O., The Gene Ontology resource: enriching a GOld mine. *Nucleic Acids Res* 2021, *49*, D325-D334.
[28] Mi, H., Muruganujan, A., Ebert, D., Huang, X., Thomas, P. D., PANTHER version 14: more genomes, a new PANTHER GO-slim and improvements in enrichment analysis tools. *Nucleic Acids Res* 2019, *47*, D419-D426.
[29] Zhou, Y., Zhou, B., Pache, L., Chang, M.*, et al.*, Metascape provides a biologist-oriented resource for the analysis of systems-level datasets. *Nat Commun* 2019, *10*, 1523.
[30] Lässig, C., Lammens, K., Gorenflos López, J. L., Michalski, S.*, et al.*, Unified mechanisms for self-RNA recognition by RIG-I Singleton-Merten syndrome variants. *Elife* 2018, *7*.
[31] Ardito, F., Giuliani, M., Perrone, D., Troiano, G., Lo Muzio, L., The crucial role of protein phosphorylation in cell signaling and its use as targeted therapy (Review). *Int J Mol Med* 2017, *40*, 271-280.
[32] Shannon, P., Markiel, A., Ozier, O., Baliga, N. S.*, et al.*, Cytoscape: a software environment for integrated models of biomolecular interaction networks. *Genome Res* 2003, *13*, 2498-2504.
[33] Wu, Y., Li, S., Role of Post-Translational Modifications of cGAS in Innate Immunity. *Int J Mol Sci* 2020, *21*.
[34] Thery, F., Eggermont, D., Impens, F., Proteomics Mapping of the ISGylation Landscape in Innate Immunity. *Front Immunol* 2021, *12*, 720765.
[35] Farber, D. L., Form and function for T cells in health and disease. *Nat Rev Immunol* 2020, *20*, 83-84.
[36] Wan, D., Jiang, W., Hao, J., Research Advances in How the cGAS-STING Pathway Controls the Cellular Inflammatory Response. *Front Immunol* 2020, *11*, 615.
[37] Steinberger, O., Lapidot, Z., Ben-Ishai, Z., Amikam, D., Elevated expression of the CD4 receptor and cell cycle arrest are induced in Jurkat cells by treatment with the novel cyclic dinucleotide 3',5'-cyclic diguanylic acid. *FEBS Lett* 1999, *444*, 125-129.
[38] Perng, Y. C., Lenschow, D. J., ISG15 in antiviral immunity and beyond. *Nat Rev Microbiol* 2018, *16*, 423-439.
[39] Villarroya-Beltri, C., Guerra, S., Sánchez-Madrid, F., ISGylation - a key to lock the cell gates for preventing the spread of threats. *J Cell Sci* 2017, *130*, 2961-2969.
[40] Zhao, C., Denison, C., Huibregtse, J. M., Gygi, S., Krug, R. M., Human ISG15 conjugation targets both IFN-induced and constitutively expressed proteins functioning in diverse cellular pathways. *Proc Natl Acad Sci U S A* 2005, *102*, 10200-10205.

[41] Campbell, J. A., Lenschow, D. J., Emerging roles for immunomodulatory functions of free ISG15. *J Interferon Cytokine Res* 2013, *33*, 728-738.
[42] Schwartz, S. L., Conn, G. L., RNA regulation of the antiviral protein 2'-5'-oligoadenylate synthetase. *Wiley Interdiscip Rev RNA* 2019, *10*, e1534.
[43] Leisching, G., Ali, A., Cole, V., Baker, B., 2'-5'-Oligoadenylate synthetase-like protein inhibits intracellular M. tuberculosis replication and promotes proinflammatory cytokine secretion. *Mol Immunol* 2020, *118*, 73-78.
[44] Leisching, G., Cole, V., Ali, A. T., Baker, B., OAS1, OAS2 and OAS3 restrict intracellular M. tb replication and enhance cytokine secretion. *Int J Infect Dis* 2019, *80S*, S77-S84.
[45] Lentine, B., Antonucci, L., Hunce, R., Edwards, J.*, et al.*, Dephosphorylation of threonine-821 of the retinoblastoma tumor suppressor protein (Rb) is required for apoptosis induced by UV and Cdk inhibition. *Cell Cycle* 2012, *11*, 3324-3330.
[46] Roskoski, R., Src protein-tyrosine kinase structure, mechanism, and small molecule inhibitors. *Pharmacol Res* 2015, *94*, 9-25.
[47] Pan, Q., Qiao, F., Gao, C., Norman, B.*, et al.*, Cdk5 targets active Src for ubiquitin-dependent degradation by phosphorylating Src(S75). *Cell Mol Life Sci* 2011, *68*, 3425-3436.
[48] Amata, I., Maffei, M., Pons, M., Phosphorylation of unique domains of Src family kinases. *Front Genet* 2014, *5*, 181.
[49] Gaud, G., Lesourne, R., Love, P. E., Regulatory mechanisms in T cell receptor signalling. *Nat Rev Immunol* 2018, *18*, 485-497.
[50] Song, B., Liu, D., Greco, T. M., Cristea, I. M., Post-translational modification control of viral DNA sensors and innate immune signaling. *Adv Virus Res* 2021, *109*, 163-199.
[51] Douglas, P., Sapkota, G. P., Morrice, N., Yu, Y.*, et al.*, Identification of in vitro and in vivo phosphorylation sites in the catalytic subunit of the DNA-dependent protein kinase. *Biochem J* 2002, *368*, 243-251.
[52] Osawa, J., Akizuki, K., Kashimura, A., Ueta, S.*, et al.*, Dual phosphorylation of protein phosphatase PPM1H promotes dephosphorylation of Smad1 in cellulo. *Biochem Biophys Res Commun* 2020, *530*, 513-519.
[53] Liu, X., Yue, J., Frey, R. S., Zhu, Q., Mulder, K. M., Transforming growth factor beta signaling through Smad1 in human breast cancer cells. *Cancer Res* 1998, *58*, 4752-4757.
[54] Ramachandran, A., Vizán, P., Das, D., Chakravarty, P.*, et al.*, TGF-β uses a novel mode of receptor activation to phosphorylate SMAD1/5 and induce epithelial-to-mesenchymal transition. *Elife* 2018, *7*.
[55] Tzavlaki, K., Moustakas, A., TGF-β Signaling. *Biomolecules* 2020, *10*.
[56] Lee, I. H., Sohn, M., Lim, H. J., Yoon, S.*, et al.*, Ahnak functions as a tumor suppressor via modulation of TGFβ/Smad signaling pathway. *Oncogene* 2014, *33*, 4675-4684.
[57] Aryal, U. K., Hedrick, V., Onyedibe, K. I., Sobreira, T. J. P.*, et al.*, Global Proteomic Analyses of STING-Positive and -Negative Macrophages Reveal STING and Non-STING Differentially Regulated Cellular and Molecular Pathways. *Proteomics Clin Appl* 2020, *14*, e1900109.
[58] Opoku-Temeng, C., Onyedibe, K. I., Aryal, U. K., Sintim, H. O., Proteomic analysis of bacterial response to a 4-hydroxybenzylidene indolinone compound, which re-sensitizes bacteria to traditional antibiotics. *J Proteomics* 2019, *202*, 103368.
[59] Mohallem, R., Aryal, U. K., Regulators of TNFα mediated insulin resistance elucidated by quantitative proteomics. *Sci Rep* 2020, *10*, 20878.
[60] Zembroski, A. S., Buhman, K. K., Aryal, U. K., Proteome and phosphoproteome characterization of liver in the postprandial state from diet-induced obese and lean mice. *J Proteomics* 2021, *232*, 104072.

[61] Cox, J., Mann, M., MaxQuant enables high peptide identification rates, individualized p.p.b.-range mass accuracies and proteome-wide protein quantification. *Nat Biotechnol* 2008, *26*, 1367-1372.
[62] Tyanova, S., Temu, T., Sinitcyn, P., Carlson, A.*, et al.*, The Perseus computational platform for comprehensive analysis of (prote)omics data. *Nat Methods* 2016, *13*, 731-740.
[63] Hornbeck, P. V., Zhang, B., Murray, B., Kornhauser, J. M.*, et al.*, PhosphoSitePlus, 2014: mutations, PTMs and recalibrations. *Nucleic Acids Res* 2015, *43*, D512-520.
[64] Miller, M. L., Jensen, L. J., Diella, F., Jørgensen, C.*, et al.*, Linear motif atlas for phosphorylation-dependent signaling. *Sci Signal* 2008, *1*, ra2.
[65] Thomas, P. D., Campbell, M. J., Kejariwal, A., Mi, H.*, et al.*, PANTHER: a library of protein families and subfamilies indexed by function. *Genome Res* 2003, *13*, 2129-2141.
[66] Wang, M., Sooreshjani, M. A., Mikek, C. Opoku-Temeng, C., Sintim, H. O., Suramin potently inhibits cGAMP synthase, cGAS, in THP1 cells to modulate IFN-β levels. *Future Med Chem* 2018, *10*, 1301-1317.